

Filamented Light (FLight) Biofabrication of Highly Aligned Tissue-Engineered Constructs

Hao Liu, Parth Chansoria, Paul Delrot, Emmanouil Angelidakis, Riccardo Rizzo, Dominic Rüttsche, Lee Ann Applegate, Damien Loterie, and Marcy Zenobi-Wong*

Cell-laden hydrogels used in tissue engineering generally lack sufficient 3D topographical guidance for cells to mature into aligned tissues. A new strategy called filamented light (FLight) biofabrication rapidly creates hydrogels composed of unidirectional microfilament networks, with diameters on the length scale of single cells. Due to optical modulation instability, a light beam is divided optically into FLight beams. Local polymerization of a photoactive resin is triggered, leading to local increase in refractive index, which itself creates self-focusing waveguides and further polymerization of photoresin into long hydrogel microfilaments. Diameter and spacing of the microfilaments can be tuned from 2 to 30 μm by changing the coherence length of the light beam. Microfilaments show outstanding cell instructive properties with fibroblasts, tenocytes, endothelial cells, and myoblasts, influencing cell alignment, nuclear deformation, and extracellular matrix deposition. FLight is compatible with multiple types of photoresins and allows for biofabrication of centimeter-scale hydrogel constructs with excellent cell viability within seconds (<10 s per construct). Multidirectional microfilaments are achievable within a single hydrogel construct by changing the direction of FLight projection, and complex multimaterial/multicellular tissue-engineered constructs are possible by sequentially exchanging the cell-laden photoresin. FLight offers a transformational approach to developing anisotropic tissues using photo-crosslinkable biomaterials.

1. Introduction


Light-based projection techniques are increasingly being used for fabrication of biomimetic tissues.^[1–3] Lately, rapid biofabrication of complex cellular architectures has been possible through tomographic projection of laser light beams.^[4–6] However, most light-guided tissue fabrication strategies have limited potential for efficient cell alignment when it comes to the creation of anisotropic tissues such as muscle and tendons,^[7,8] because most approaches focus on macrofeatures (>100 μm) that lack the topographical cues necessary for the highly aligned cellular and extracellular organization found in these tissues. For techniques such as two-photon polymerization and ultrahigh resolution digital light processing that can achieve cell-scale (<30 μm) resolution, the incoherent light sources restrict the photopolymerization occurring in a small range ($<\text{mm}$), which needs layer-by-layer strategies to achieve fabrication of large tissue-engineered constructs.^[1,9,10] The compromise on speed and scalability limits the translational potential of these

approaches. Instructive guidance cues (e.g., fiber components and a combination of fiber and extrusion-based bioprinting) have been widely studied for their potential to advance cell alignment and maturation of aligned tissue-engineered constructs, such as muscle, tendons, nerves, and cartilage tissues.^[7,11–14] Topological cues with an increased aspect ratio have been shown to affect the bioactivity of cells in/on the substrate. For example, the rod-shaped microgels (aspect ratio of 10) fabricated by microfluidics or soft lithography are able to increase cell orientation, which is better achieved through the void between high-aspect-ratio microrods compared to microspheres.^[15,16] Topological features with ultrahigh aspect ratio ($>20:1$) created by micropatterning techniques can effectively induce cell adhesion and alignment.^[17,18] Especially when the dimensions of the confinement approach the scale of the cell nucleus (<10 μm), nuclear deformation resulting from these longitudinal confinements becomes apparent. The elongated shape of the cell nucleus can influence cell differentiation, gene expression, and rejuvenation, the latter by chromosome reorganization and activation of DNA repair mechanisms;^[19,20]

H. Liu, P. Chansoria, E. Angelidakis, R. Rizzo, D. Rüttsche, M. Zenobi-Wong
Tissue Engineering + Biofabrication Laboratory
Department of Health Sciences & Technology
ETH Zürich
Otto-Stern-Weg 7, Zürich 8093, Switzerland
E-mail: marcy.zenobi@hest.ethz.ch

P. Delrot, D. Loterie
Readily3D SA
EPFL Innovation Park
Lausanne 1015, Switzerland

L. A. Applegate
Regenerative Therapy Unit, Plastic, Reconstructive & Hand Surgery
Lausanne University Hospital
University of Lausanne
Epalinges 1066, Switzerland

 The ORCID identification number(s) for the author(s) of this article can be found under <https://doi.org/10.1002/adma.202204301>.

© 2022 The Authors. Advanced Materials published by Wiley-VCH GmbH. This is an open access article under the terms of the Creative Commons Attribution License, which permits use, distribution and reproduction in any medium, provided the original work is properly cited.

DOI: 10.1002/adma.202204301

and a change to a rounder nuclear shape can be associated with disease pathology.^[21] At the tissue level, a more elongated cell nucleus (aspect ratio of 2.5–6) can be observed in anisotropic tissues like tendons, compared to isotropic tissues (1.1–1.8).^[22] A high aspect ratio of the nucleus in tenocytes is contributed to maintaining the phenotype of tenocytes and the expression of key genes during aging.^[23] However, none of the above techniques provide topological cues for both cell alignment and nucleus deformation in a 3D environment.

In this work, we show that the phenomenon of optical modulation instability (OMI)^[10,24] of filamented light beams inside a photoresin can be advantageously employed for the fabrication of highly aligned hydrogel microfilaments ($\Phi < 30 \mu\text{m}$) inside macrosized ($L \geq 10 \text{ mm}$, $\Phi \geq 3 \text{ mm}$) hydrogel constructs. To the best of our knowledge, this is the first use of OMI for the biofabrication of highly aligned tissue-engineered constructs. OMI is defined as the spontaneous break-up of a uniform optical beam into filamented light beams while propagating within optical nonlinear media. Photoreactive polymers are well-known optically nonlinear media, since their photopolymerization rate and thus their refractive index (RI) change depend on the intensity of the crosslinking light.^[25–27] Unidirectional microfilament networks are generated by shining a partially spatially coherent light beam into a resin-containing vial. Upon incidence of the filamented light beam onto the hydrogel interface, microfilaments are seeded by local intensity maxima of the incident light beam. Each local maximum intensity of light offers a faster crosslinking rate, thus creating a local maximum RI. In turn, local RI maxima act as optical traps, resulting in the propagation of the whole micropatterned polymerization front through the volume of resin via these self-focusing waveguides, which leads to the permanent recording of light filamentation. At the same time, local minima of light intensity are distributed among the localized light beams, corresponding to the formation of void spaces where local intensity is below the threshold required for polymerization. These voids between microfilaments are presented as channel-like void spaces (microchannels) with ultrahigh aspect ratios after the removal of uncrosslinked photoresin.

Here, we present a biofabrication strategy for highly aligned tissue-engineered constructs called filamented light (FLight) biofabrication, in which highly aligned microfilaments are induced by the OMI, which is caused by the interaction of spatially coherent light beams with a variety of photoresin compositions. Cells are rapidly (<10 s) and safely encapsulated into hydrogel matrix containing unidirectional microfilament networks. This approach meets the requirements for engineering biomimetic anisotropic tissues, including instructive guidance cues at microscale resolution and fast and cell-friendly processing. In the FLight biofabrication, the dimension of microfilaments and the void spaces between the microfilaments are tunable and on the same length scale as cells; this provides efficient cell guidance properties and supports cell migration through the interfilament void spaces.

Our strategy provides control of the fabricated hydrogel constructs at the micro- and macrolevel, i.e., control over the dimension (2–30 μm) and direction of microfilaments, and over the size, shape, and material composition of projected tissue-engineered constructs. These advantages offer flexibility in the

biofabrication of cell-laden hydrogel structures, such as multihollow/tubular hydrogel structures which have been shown to improve cell viability prior to vascularization as previously studied.^[28,29] In addition, we show FLight can be efficiently utilized for multicellular/multimaterial biofabrication. Using the multicellular/multimaterial FLight process, (bio)photoresins can be cured at desired locations to create complex tissue constructs that better mimic the hierarchical organization of native tissues, such as muscle.^[7] Hydrogel constructs containing multiple directional microfilaments can be achieved by performing the FLight process from different directions (Cross-FLight), which is promising for biofabrication of anisotropic tissues such as the myocardium.^[30,31] Finally, we demonstrate the ability to fabricate larger hydrogel constructs (approximately cm) by multiple step FLight strategy (Multi-FLight), in which single hydrogel constructs can be stacked on top of each other to result in a long hydrogel construct featuring microfilaments throughout its length for cell guidance and alignment. This also allows for gradient control over the direction of the microfilaments, including different materials and varying physical properties of the microfilaments, thus enabling the biofabrication of human-sized muscle engineered constructs and complex interfaces (i.e., muscle–tendon junction), incorporating multiple distinct morphologies/microstructures/cell types.^[32]

2. Results and Discussion

2.1. Optical Modulation Instability and Self-Focusing Induce Unidirectional Microfilament Networks

The physical phenomenon behind FLight's ability to form cell instructive hydrogel microfilaments from photosensitive resins is illustrated in **Figure 1a**. The projected light beam features intensity noise patterns that translate into unidirectional microfilament networks which make up the hydrogel structures. First, we highlight the physics that gives rise to the formation of these microfilaments within the photoresins. **Figure 1b** illustrates the relative change of RI and light intensity mapping at the interface between photoresin and cuvette at different time points. The image projected onto the transparent photoresin-containing cuvette features a speckle-pattern intensity noise originating from the spatial coherence of the input light source. This small intensity noise is then nonlinearly amplified by the crosslinking of photoresin, resulting in microscopic resin waveguides that propagate the filamented light beam front through the resin volume (i.e., cuvette inner thickness). More specifically, the initial local intensity noise maxima locally crosslink the photoresin from cuvette–photoresin interface, thus inducing a localized increase of RI in the photoresin. In turn, the photoresin RI changes result in a self-focusing effect at the interface between crosslinked and uncrosslinked photosensitive material in the *z*-direction. The formation of local RI maxima also creates local microwaveguides which optically trap the incident light beam front and propagate into the photoresin over a long distance. In other words, the trapped and focused light beams further crosslink the photoresin, thus continuously inducing the self-focusing effect and creating long microfilaments within seconds. The cumulative effect of multiple local

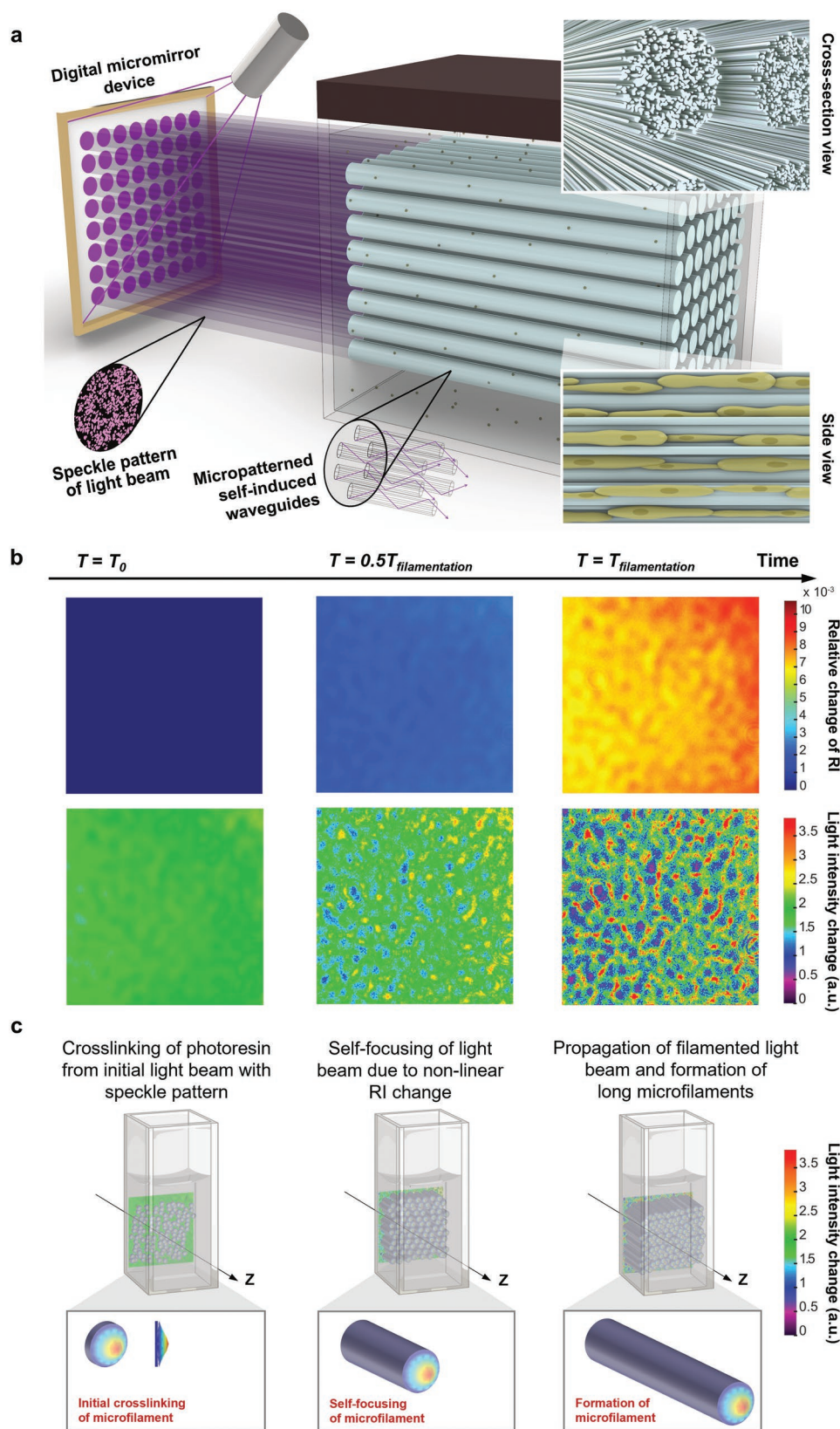


Figure 1. FLight biofabrication strategy of hydrogel constructs containing highly aligned microfilaments with efficient cell guidance properties. a) Schematic illustration of FLight strategy for fabricating highly aligned microfilaments and their cell guidance properties. b) Physics of the FLight process showing relative refractive index (RI) change of the photoresin (top) and light intensity mapping (bottom) at different time points. These maps show

intensity maxima in proximity to each other produces microfilaments in the created hydrogel constructs. Furthermore, low intensity is distributed between the local maxima as the pattern indicated in the intensity map, which leads to slightly crosslinked parts between the microfilaments (Figure S1, Supporting Information). The hydrogel microfilaments and the slightly crosslinked parts form unidirectional microfilament networks, ensuring the stability of the entire hydrogel constructs. However, such slightly crosslinked parts are not occupied between all of the microfilaments. The uncrosslinked photoresin between the microfilaments is still present due to the local minima of intensity noise during the FLight process, leaving behind ultrahigh-aspect-ratio microchannels in the unidirectional microfilament networks after washing (Figure 1c). It is important to note that spatial coherence in the incident light can be optically tuned, while generation and propagation of microfilaments are dependent upon optical nonlinearity properties of the resin (i.e., RI changes upon photo-crosslinking), thus altering characteristics of the microfilaments. In the next section, we discuss how the dimensions of the microfilaments from different photoresins can be tuned.

2.2. Hydrogel Microfilaments for Cell Guidance are Highly Aligned and Tunable in Dimension

FLight biofabrication was demonstrated using several photosensitive resins based on chain-growth and step-growth polymerizations.^[5,34] Due to the excellent kinetics of the norbornene-thiol reaction, microfilaments were able to be formed within seconds, thus minimizing potential cell damage from photo-crosslinking and allowing for the use of low polymer concentrations. We first produced hydrogel samples using Gel-NB/4PEG-SH photoresin. The critical light dose for FLight process was determined by performing a light dose test based on our previous work.^[5] For the 2.88% w/v Gel-NB/4PEG-SH photoresin, a light dose of 195 mJ cm⁻² was used to create a FLight hydrogel construct with high fidelity to the designed dimensions (Figure S2 and Table S1, Supporting Information). A 1 mm diameter hydrogel cylinder was projected (Figure 2a) and the formation of microfilaments (diameter of 9.8 ± 2.5 μm) within the hydrogel cylinder was confirmed (Figure 2b). Here, ≈88% of the microfilaments were parallel (-1° to 1°) to the projection direction (Figure 2c).

Since the generation of microfilaments is dependent on spatial coherence of the light beams and nonlinear media, we tested FLight using a higher concentration of Gel-NB/4PEG-SH (5% w/v), as well as other common photosensitive biomaterials (gelatin methacryloyl (Gel-MA), hyaluronic acid methacrylate

(HA-MA), and alginate methacrylate (Alg-MA)) (Figure 2d). Microfilaments were formed using all photoresins, with highly aligned microfilaments in all cases (>86%, -1° to 1°). The projection dose varied from 180 to 5650 mJ cm⁻² depending on the resin, as did the diameter of the microfilaments (8.1 ± 1.4 to 11.1 ± 3.1 μm) (Figures S3 and S4 and Table S1, Supporting Information).

High-aspect-ratio structures can offer cell guidance, and the ability to tune their dimensions would make FLight applicable to a broad range of aligned tissues having extracellular matrix (ECM) fibers ranging from 1 to 100 μm.^[35,36] Here, microfilaments with varying diameter ranges were fabricated by adjusting the spatial coherence length using a standard Köhler illumination system consisting of a 405 nm light-emitting diode light source.^[37] Specifically, this light-induced self-organization depends on spatial coherence of the light source and strength of the photoreactive material's RI nonlinearity.^[26] The more spatially coherent the light beam (i.e., the longer the spatial coherence length l_c of the light beam), the broader the diameter of the microfilaments. In the Köhler illumination system, the spatial coherence length of the light beam could be extended between the theoretical range of 3.7 and 25.8 μm (Figure S5a, Supporting Information) by adjusting the aperture diameter (AD). This range of spatial coherence length allowed us to control the diameters of microfilaments between 8.3 and 17.8 μm using 5% w/v Gel-NB/4PEG-SH photoresin (Figure 2e). The mean diameters of microfilaments made from methacryloyl resins were 5.0 to 13.6, 2.4 to 8.3, and 4.7 to 13.7 μm using 5% w/v Gel-MA, 2% w/v HA-MA, and 2% w/v Alg-MA photoresins, respectively. However, the mean diameter of microfilaments was found to be independent of the field diameter of our Köhler system (Figure S5b,c, Supporting Information), which further demonstrates that the spatial coherence of the light beams induced by OMI controls the formation of microfilaments and that the microfilaments' diameter is tunable by adjusting the spatial coherence length of the light beam.

Due to the reinforcing effect of the unidirectional microfilament networks,^[38,39] the FLight hydrogel constructs exhibit ideal mechanical properties for tissue engineering applications. Mechanical stimulation can be applied to FLight hydrogel constructs, which further induces cell alignment and boosts tissue maturation.^[13,40,41] Bulk hydrogel and FLight hydrogel samples were fabricated using Gel-NB/4PEG-SH or Gel-MA photoresin for tensile and compressive tests (Figure 2f,g and Figure S6, Supporting Information). When the tensile tests were performed in the direction parallel to the microfilaments ("||," along the long axis of microfilament), the yield stress of hydrogel samples prepared using 2.88% w/v Gel-NB/4PEG-SH photoresin increased from 2.7 kPa (bulk hydrogel) to 6.0 kPa

the changes that occur in the photoresin near the interface of the photoresin-cuvette. In the initial stage ($T = T_0$), the photoresin RI is homogenous, since crosslinking has not yet begun. However, the nonhomogenous light intensity distribution (speckle noise as shown in the intensity map) leads to the initial local crosslinking of the photoresin from the local intensity maxima. At $T = 0.5T_{\text{filamentation}}$, the locally crosslinked photoresin situated at the local intensity maxima has an increased RI compared to uncrosslinked photoresin, which results in self-focusing of the incident light beam. This self-focusing effect causes a continuous growth of local RI maxima through the photoresin volume, thus guiding and propagating the light beam. Finally, the original nonhomogenous distribution of light intensity is nonlinearly amplified and integrated by the resin as microfilaments ($T = T_{\text{filamentation}}$), due to the self-focusing effect of light beams. The simulation of RI change in photoresin and light intensity mapping was generated using a BPM tool described in a previous study.^[33] c) Long and continuous microfilaments and microchannels are generated in anisotropic hydrogel constructs that correspond to the local maximum and minimum of light intensity.

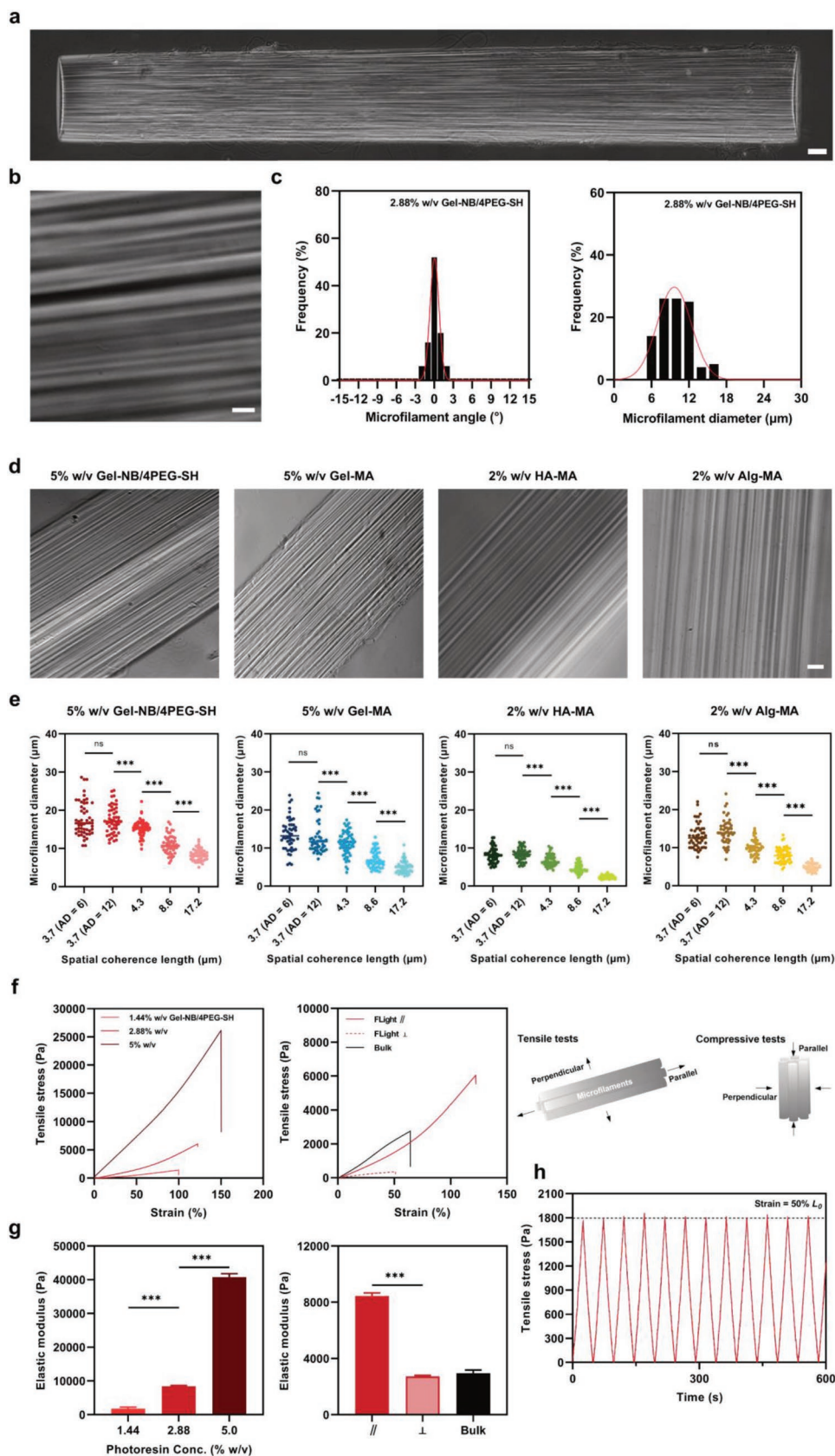


Figure 2. Characterization of FLight hydrogel construct containing microfilaments. a) Bright-field image of entire 1 mm-diameter and 7 mm-long FLight hydrogel construct created using 2.88% w/v Gel-NB/4PEG-SH photoresin. Scale bar: 200 μm . b) Magnified image of microfilaments structuring of the

(FLight hydrogel), and yield strains increased from 64% to 122%. Similar results were found in the hydrogel samples produced using 5% w/v Gel-MA photoresin, wherein, the yield stress and yield strain (in the direction parallel to the microfilaments) were found to be 1.8 kPa and 36% in the bulk hydrogel sample, but increased to 7.8 kPa and 105%, respectively. Interestingly, we also confirmed the anisotropy in the mechanical properties of FLight hydrogel constructs. The yield stress and yield strain of FLight hydrogel samples prepared using 2.88% w/v Gel-NB/4PEG-SH decreased to 0.4 kPa and 51%, when the tensile loadings were applied in the direction perpendicular to the microfilaments (\perp). The FLight hydrogel constructs fabricated using 5% w/v Gel-MA also showed decreased tensile properties (1.1 kPa, 81%) in the perpendicular position compared to the parallel position. The compressive elastic modulus of cylindrical FLight hydrogel constructs (a diameter of 5 mm and a height of 4 mm) in the direction parallel to the microfilaments increased from 1.8 to 40.7 kPa, when increasing Gel-NB/4PEG-SH photoresin concentration from 1.44% to 5%. Likewise, the compression of FLight hydrogel samples revealed a higher elastic modulus in the parallel position compared to the perpendicular position; 8.4 kPa versus 2.7 kPa for 2.88% w/v Gel-NB/4PEG-SH and 15.8 kPa versus 1.9 kPa for 5% w/v Gel-MA photoresins, respectively. These anisotropic mechanical properties can be explained by the lower crosslinking of materials, which is consistent with the description of the unidirectional microfilament networks, i.e., the presence of slightly crosslinked parts between microfilaments; and the failure occurs first from these parts when mechanical force is applied in a direction perpendicular to the microfilaments. Moreover, the deformation recoverability of the FLight hydrogel constructs was investigated by cyclic loading–unloading tests as shown in Figure 2h and Video S1 in the Supporting Information. No residual strain was generated after loading–unloading during 10 min of stretching at a tensile strain of 50% in the air condition, which suggests that hydrogels containing microfilaments did not undergo plastic deformation upon tensile loading.

2.3. Channel-Like Voids Guide Anisotropic Cell Migration in FLight Hydrogel Matrix

The nanoscale pore size of conventional hydrogel networks hinders the diffusion of oxygen and nutrients and lacks cell guidance cues. Micrometer-scale interconnected void spaces should be present in an ideal tissue engineering matrix, to provide 3D

spaces for cell migration, proliferation, vascularization, and ECM deposition.^[42–44] A large fraction of the FLight hydrogel matrix is occupied by microchannels with ultrahigh aspect ratio (>700:1). These microchannels offer void spaces into which the cell can migrate, causing alignment of the cell and its nucleus. The FLight hydrogel construct containing fluorescent-labeled microfilaments was created using 5% w/v fluorescent-labeled Gel-MA photoresin with subsequent washing of uncrosslinked photoresin. A large number of microchannels were observed among the unidirectional microfilament networks, as highlighted in **Figure 3a** (see also Video S2, Supporting Information). The void fraction was found to be about 50% in the whole FLight hydrogel volume, which is independent of the spatial coherence length of light beams (Figure 3b). Microchannels were homogeneously distributed within the hydrogel volume by measuring the ratio of microfilaments/microchannels for each layer in the 3D confocal images (Figure 3c and Figure S7, Supporting Information).

The physical limitation provided by pores smaller than 3 μm has been shown to significantly restrict cell migration in a 3D tissue matrix.^[45] This size is considered to be the threshold through which cells cannot pass, due to the limited deformability of the nucleus. Here, the diameter of microchannels was tuned by adjusting the spatial coherence length of light beam to ensure effective cell migration through the microchannels. The mean diameter of the microchannels was increased from 2.7 to 5.8 μm when decreasing the coherence length from 172 to 3.7 μm using 5% w/v fluorescent-labeled Gel-MA (Figure 3e). Meanwhile, the mean aspect ratio of microchannel structures decreased from 1540:1 to 700:1, with increases in the spatial coherence length (Figure 3f). To achieve cell migration and a higher aspect ratio for efficient cell guidance, normal human dermal fibroblasts (NHDFs) were encapsulated in FLight hydrogels containing microchannels with an average diameter of 3.5 μm and an aspect ratio of 1178:1. The NHDFs were stained by calcein-AM to evaluate their morphology after 1 h, 1, 3, and 7 days of culture. In the FLight biofabrication process, the light beams penetrated the cells and crosslinked the photoresin on both sides of cell, which is defined as the original encapsulation site. Already after 1 h the spreading of NHDFs was observed, accompanied by an elongated morphology of cells and a deformed nucleus near the original encapsulation site (highlighted by yellow arrows in Figure 3d and Video S3, Supporting Information). The mean aspect ratio of cells was increased from 1.24 to 15.8 after 7 days of culture (Figure 3g), which demonstrates the elongation of cells. Furthermore, an

hydrogel sample. Scale bar: 20 μm . c) Distribution of the microfilament diameter, and the distribution of angles' difference between the orientation of microfilament and direction of projection (all data were collected from BF images, $n = 3$). d) Bright-field images of microfilaments in FLight hydrogel constructs fabricated using 5% w/v Gel-NB/4PEG-SH, 5% w/v Gel-MA, 2% w/v HA-MA, and 2% w/v Alg-MA photoresin. Scale bar: 50 μm . e) Diameter of microfilaments under different spatial coherence lengths by adjusting the AD using a standard Köhler illumination system ($n = 3$). f) Left: Tensile mechanical properties of FLight hydrogel constructs using different concentrations of Gel-NB/4PEG-SH photoresin. The mechanical loadings were applied parallel to the microfilaments (\parallel). Right: Tensile tests of FLight hydrogel constructs in the parallel direction, in the perpendicular direction of microfilaments (\perp), and bulk hydrogels using 2.88% w/v Gel-NB/4PEG-SH photoresin. FLight and bulk hydrogel samples were produced as hydrogel strands 12 mm long and 1 mm in diameter for tensile testing. g) Left: Compressive moduli calculated from the stress–strain curves obtained from hydrogel samples prepared using 1.44% w/v, 2.88% w/v, and 5% w/v of Gel-NB/4PEG-SH photoresin. The mechanical loading was applied parallel to the microfilaments (\parallel). Right: Elastic modulus of FLight hydrogel constructs in the parallel direction, in the perpendicular direction of microfilaments (\perp), and bulk hydrogels using 2.88% w/v Gel-NB/4PEG-SH photoresin. Hydrogel samples for compressive testing were prepared as cylinders with a diameter of 5 mm and a height of 4 mm, $n = 3$. h) Cycle loading–unloading tensile curve of hydrogel sample prepared using 2.88% w/v Gel-NB/4PEG-SH photoresin. The test was performed in air conditions with a target strain of 50% in the parallel direction of microfilaments.

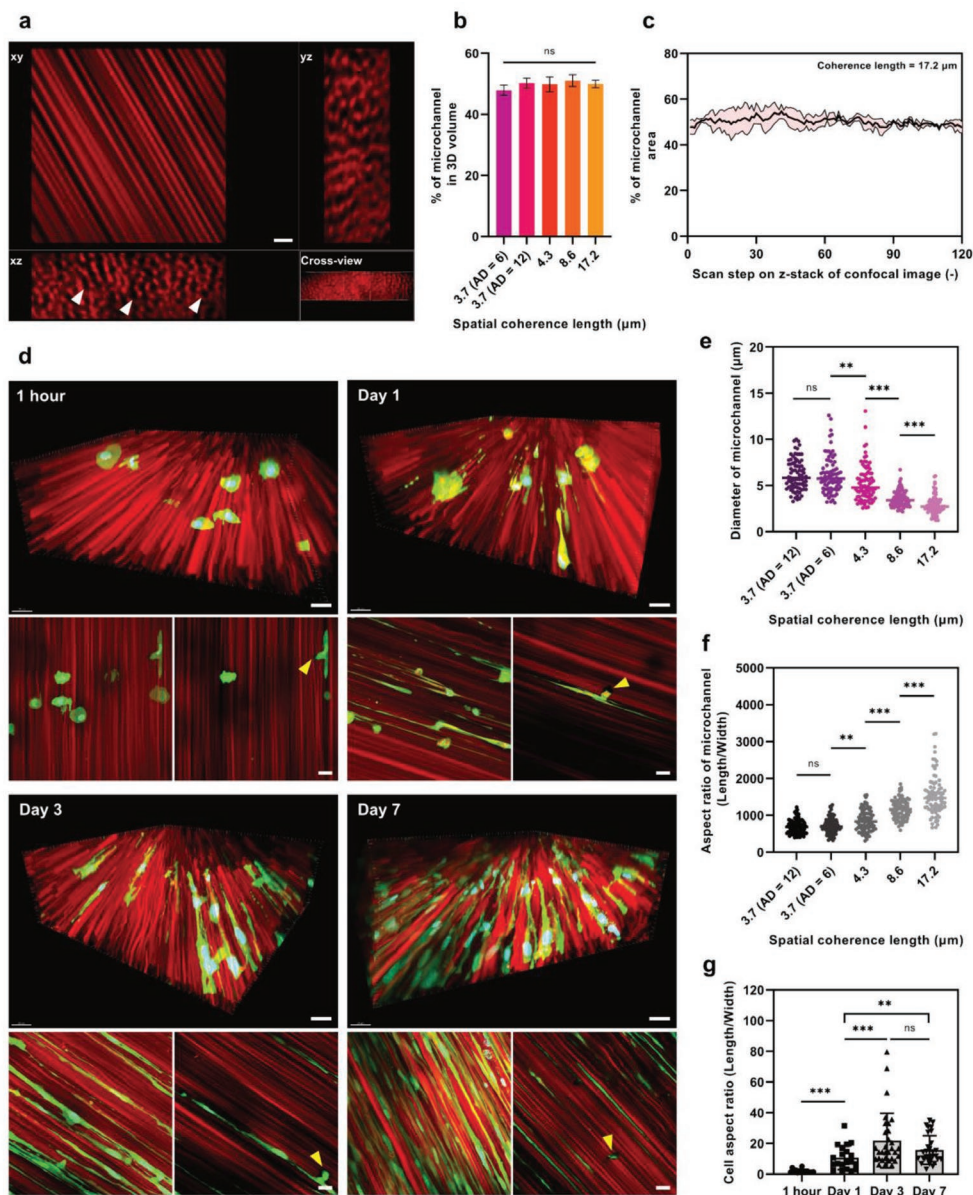


Figure 3. Microchannels present in the FLIGHT hydrogel matrix support cell migration. a) Projected image of unidirectional microfilament networks in FLIGHT hydrogel matrix produced using 5% w/v fluorescent-labeled Gel-MA photoresin. The white arrows indicate the microchannels between microfilaments after washing. Scale bar: 20 μm . b) Percentage of microchannels in 3D hydrogel volume created with varying spatial coherence length. All data were measured from 3D confocal fluorescence images using Imaris software ($n = 3$). c) The ratio of void area in each scan step on z-stack of confocal fluorescence images (data collected using ImageJ), 120 steps in the z-direction, 0.5 μm distance between steps). d) Fluorescence images of cell-laden hydrogel matrix. Nuclei and NHDFs were stained by Hoechst 33342 and Calcein-AM after 1 h, 1, 3, and 7 days of culture. At each time point, the bottom left panels are projected images (max intensity) and the bottom right panels are single, sliced images. The yellow arrows highlight the original encapsulation site of fibroblasts after FLIGHT process. Scale bars: 20 μm . e) Mean diameter of microchannels in FLIGHT hydrogel constructs produced by light beams with different spatial coherence lengths using 5% w/v fluorescent-labeled Gel-MA photoresin. The diameter was measured as the distance between microfilaments in fluorescence images. The microchannel was randomly selected from eight different z-steps of confocal images (10 data per z-step). f) Mean aspect ratio of microchannels in hydrogel constructs fabricated with varying coherence lengths of the light beam ($n = 3$). g) Cell aspect ratio at different time points. All data were collected from fluorescence images ($n = 3$).

increasing number of encapsulated fibroblasts occupied the void spaces between the microfilaments, which may be due to cell migration. Interconnectedness of the microchannels of the FLIGHT hydrogel matrix (e.g., cells can migrate through interconnected microchannels) was confirmed by the cell migration in two directions: in a perpendicular direction and

a parallel direction to the microchannels. Fibroblasts were first post-seeded on the surface of FLIGHT hydrogel matrix or bulk hydrogel constructs, and the migration depth from the surface was measured to evaluate their migration in a perpendicular direction. Fibroblasts on the surface of FLIGHT hydrogels were observed to migrate into the hydrogel matrix after 1 day

of incubation, but not from the surface of bulk hydrogels. The significant differences in cell migration depth show that these microchannels are interconnected to allow cell migration in a perpendicular direction to the microchannels (Figure S8a,b, Supporting Information). Next, by performing the FLight bio-fabrication in a container containing two types of photoresin, a hydrogel construct containing different matrix compositions in the direction of the microfilaments can be achieved. The fibroblasts were encapsulated in the cell-laden zone and the migration of fibroblasts to the cell-free zone in the direction parallel to the microchannels was investigated. After 3 days of culture, the presence of fibroblasts/nuclei in the cell-free zone was confirmed, which indicated that the encapsulated cells can migrate in the parallel direction to the microfilaments via the continuous microchannels (Figure S8c, Supporting Information).

Overall, the above results demonstrate that these continuous, interconnected microchannels between the microfilaments can support cell migration in the directions both parallel and perpendicular to microchannels. Such cell migration is essential for establishing cell–cell contact in a 3D matrix, such as the 3D network of tenocytes that requires gap junction-mediated intercellular communication.^[46] Moreover, microchannels can induce elongation of cells and support the nuclear migration, contributing a critical action in maintaining cell phenotypes and accelerating the fusion of myoblast for cellular reconstruction after muscle physiological damage.^[47]

The regulation of gene expression resulting from reorganization of the nucleus upon mechanical confinement has shown interesting results in the tissue engineering field. For example, nuclear confinement can induce redifferentiation and reprogramming of cell fate by activating DNA repair pathways.^[19,20,48] At the tissue level, gene expression associated with ECM production is upregulated in cells with elongated nuclei under dynamic mechanical loading.^[19,49,50] In this study, we demonstrated that ultrahigh-aspect-ratio microchannels have unique advantages for creating highly aligned tissue-engineered constructs by inducing mechanical confinement. Different tissue microenvironments were created using the same bioresin formulation (2.88% w/v Gel-NB/4PEG-SH photoresin with NHDFs), including the 3D FLight hydrogel, 3D bulk hydrogel, and 2D FLight hydrogel. The cells were encapsulated in the hydrogel construct containing 3D FLight hydrogel, in the bulk hydrogel, or post-seeded onto the surface of microfilaments (2D FLight hydrogel). The alignment of cells under different conditions was determined by phalloidin staining after 1 h, 1, 3, and 7 days of culture (Figure 4a). The cells started aligning in the direction parallel to the microfilaments after 1 day of incubation in both 3D and 2D FLight conditions, but not in bulk hydrogel, which again demonstrated the cell guidance property of microfilaments as physical cues. Compared to 2D FLight, NHDFs encapsulated within the 3D FLight matrix exhibited a lower proliferation level (ratio of Ki67 positive cells) on the first day. However, ≈76% of the NHDFs were found to be Ki67-positive cells after 3 days of culture, while this ratio was about 19% on the surface of FLight hydrogel matrix (Figure 4b). Similar results have been reported on rejuvenating and proliferating states of fibroblasts after static compressive force and laterally restricted culture.^[51,52] The mechanical confinement obtained from the hydrogel matrix could offer a new way to induce cell

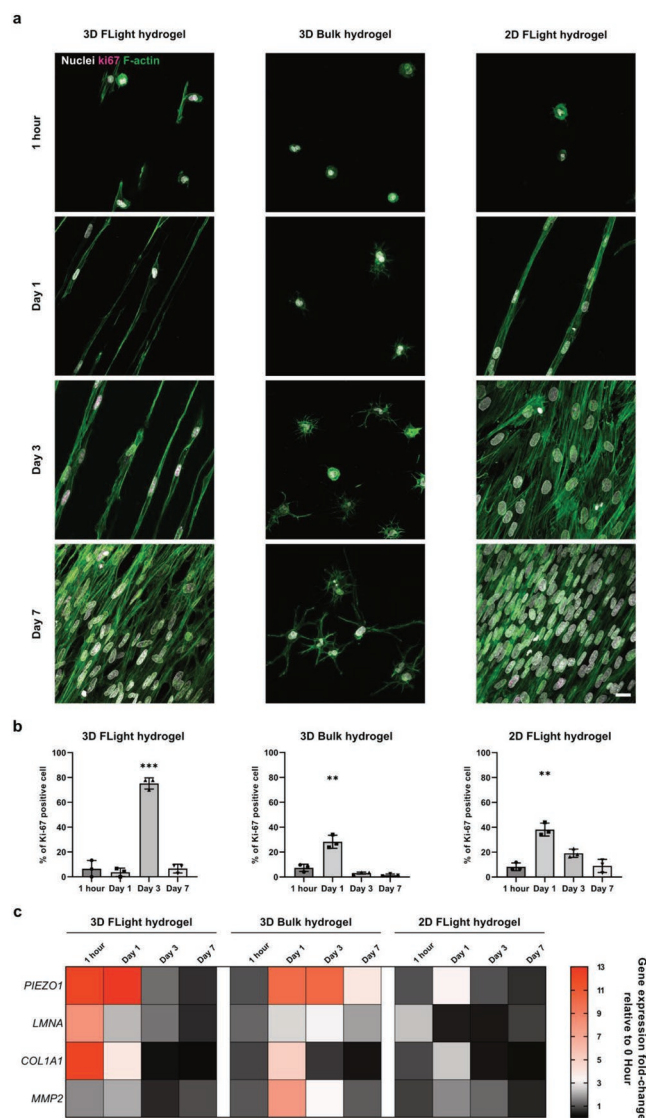


Figure 4. Microchannels provide mechanical confinement to increase proliferation and collagen formation. a) Immunofluorescence staining of Ki67 in hydrogel samples fabricated from different strategies after 1 h, 1, 3, and 7 days of culture. Scale bar: 20 μ m. b) Ratio of Ki67 positive cell in hydrogel samples at different time points. All data were calculated using ImageJ ($n = 3$). c) Relative change of gene expressions in cell-laden (3D FLight, bulk)/cell-seeded (2D FLight) hydrogel constructs after 1 h, 1, 3, and 7 days of culture. The fold change given in the heat map is the mean value. All data were collected from three biological replicates of hydrogel samples (with two technical replicates per sample).

proliferation, especially for aged cells with proliferation deficits, such as tenocytes and tendon stem/progenitor cells.^[53,54]

Next, we demonstrated that ultrahigh-aspect-ratio microchannels and the resulting cell confinement can regulate gene expression (Figure 4c and Figure S9, Supporting Information). Upregulation of the mechanosensitive ion channel Piezo1 was found at the initial stage (1 h and 1 day) in 3D FLight hydrogel (i.e., cells encapsulated within the hydrogel), compared to the 3D bulk hydrogel and 2D FLight hydrogel (i.e., cells post-seeded on the surface). Similarly, we observed an upregulation of Lamin A/C protein expression (encoded by *LMNA* gene) in

3D FLight hydrogel at 1 h; this gene has integral roles in the transduction of mechanical signals from the cell membrane into the nucleus and in nuclear stiffness.^[20,55] Furthermore, *COL1A1* expression was upregulated at the beginning of incubation, similar to *PIEZO1* expression. Earlier studies have demonstrated the relevance of *PIEZO1* to the gene expression associated with ECM production. For example, the lack of *PIEZO1* leads to a decrease in *COL1A1* expression, and *PIEZO1* plays a critical role in ECM deposition during tissue maturation under mechanical stimulation, such as tensile loading.^[56–59] Also, the lack of these micrometer-sized voids in bulk hydrogel leads to higher *MMP2* expression levels to aid cell migration by remodeling the hydrogel matrix.^[60] However, the decrease in *PIEZO1* was found from day 3, which could be explained as a loss of mechanical confinement. The change in the dimension of microchannels may be caused by the deformation of microfilaments during cell contracting, thus reducing the physical confinement on nuclei.^[61,62] In our future work, we plan to offset this loss of mechanical confinement by applying additional static/dynamic tensile loading, which is also critical for the biofabrication of matured anisotropic tissues.^[63]

2.4. FLight Biofabrication of Highly Aligned Tissue-Engineered Constructs

We demonstrated the ability of FLight to biofabricate highly aligned tissue-engineered constructs using 2.88% w/v Gel-NB/4PEG-SH photoresin with four cell types: NHDFs, human tenocytes (HTs), human umbilical vein endothelial cells (HUVECs), and mouse myoblasts (C2C12). Cell viabilities were found to be above 85% for all cell types 1 h after FLight biofabrication. By contrast, low cell viability of HUVECs (<70%) was observed in bulk hydrogels, which were prepared using the same light dose as FLight (Figure S10, Supporting Information). However, when the incubation was extended to 21 days, the viability of C2C12 was about 74% in the FLight hydrogel samples. To overcome this limitation, a series of hollow microstructures several hundred micrometers in diameter was created in FLight hydrogel constructs by blocking light from the designed projection image. The encapsulated C2C12 cells showed higher cell viability (~89%) in hydrogel constructs containing multiple hollow channels after 3 weeks of culture. Therefore, multihollow microstructures (diameter of 216 μm) were employed in subsequent experiments to achieve higher bioactivity in cell-laden hydrogel constructs.

The potential of FLight biofabrication in engineering anisotropic tissues is based on the microstructures' ability to guide cell alignment and on the alignment of ECM (i.e., self-aggregation into aligned collagen fibers). Using NHDFs, the cell-guiding property of the microfilaments was tested in structured samples with a diameter of about 1 mm (light exposure 2.8 s, containing multihollow microstructures). Phalloidin staining was used to visualize the capability of microfilaments to guide cell alignment (Figure 5a). 99% of the NHDFs were elongated and aligned within $\pm 30^\circ$ of the direction parallel to the microfilaments during the 14 days of culture (Figure 5e and Figure S11a, Supporting Information). The formation of aligned collagen type I was confirmed from the immunofluorescence images

using an anticollagen type I antibody (Figure S11b–e, Supporting Information). On the other hand, no cell alignment and aligned collagen fibers were found in the bulk hydrogels due to a lack of cell-guiding cues (Figure S12a–c, Supporting Information). Similarly, more collagen-positive areas (~48%) were found in FLight hydrogel than in the bulk hydrogel (~28%), as shown in Figure 5f. Interestingly, cell nuclei were also elongated and orientated in the FLight hydrogel constructs compared to nuclei of randomly orientated fibroblasts in the bulk hydrogel sample (Figure 5g and Figure S12d,e, Supporting Information). Recent studies have shown that physical cues can regulate the shape of cells and nuclei, ultimately affecting the phenotype, cell behavior, and gene expression. For example, the presence of fiber components in tissue matrices can induce fibroblasts to switch their phenotype to a myfibroblastic state, characterized by elongated shape.^[50] Furthermore, laterally restricted cultures of fibroblasts induce de-differentiation and reprogramming, which leads to rejuvenation of aged fibroblasts.^[51,64]

Next, we studied the alignment of HTs in hydrogel matrix fabricated by FLight, which has important implications for the biofabrication of tendon tissue models. Highly aligned filamentous actins (F-actin) were found in HTs after 2 weeks of culture. Immunofluorescent detection of type I collagen fibers again demonstrated that the microfilaments provide efficient guidance for cells and their deposited ECM (Figure 5b). Additionally, by introducing a fibroblast-HUVEC co-culture system, we showed that the formation of highly aligned blood capillaries could also be guided by FLight technique as detected by CD31 immunostaining in 2 weeks cultures (Figure 5c). Interestingly, we found the continuous capillaries to be aligned in the direction parallel to microfilaments, and some vasculatures were observed with a length >1.4 mm. Blood capillaries were confirmed to have lumen, as seen from a cross-sectional view of the 3D confocal image (Figure S13, Supporting Information).

Finally, C2C12 cells were encapsulated in 2.88% w/v Gel-NB/4PEG-SH photoresin and FLight was performed to further demonstrate its potential in the biofabrication of muscle tissue-engineered constructs. Upon exposure to differentiation medium containing 2% v/v horse serum, we observed the fusion of myoblasts and alignment of myotubes as seen with immunofluorescence staining using antimouse myosin heavy chain (MyHC) antibody and phalloidin after 3 weeks of culture (Figure 5d). 95% of myotubes were found to be aligned in the parallel direction of microfilaments (-30° to 30°) within the FLight tissue-engineered constructs (Figure 5h). As expected, the myotubes showed a random orientation in the bulk hydrogel. Similarly, more highly aligned contractile myotubes with a higher fusion index were found in FLight hydrogel constructs compared to bulk hydrogels (Figure 5i and Video S4, Supporting Information). It was interesting to observe that over 76% of the myotubes in FLight tissue-engineered constructs had more than six nuclei per myotube (Figure 5j), which were not found in the bulk hydrogel samples.

Overall, we have demonstrated that FLight is an effective strategy for the biofabrication of highly aligned tissue-engineered constructs, with rapid manufacturing times and excellent cell biocompatibility. The cell-guiding physical cues, microfilaments, lead to efficient alignment of cells required to create

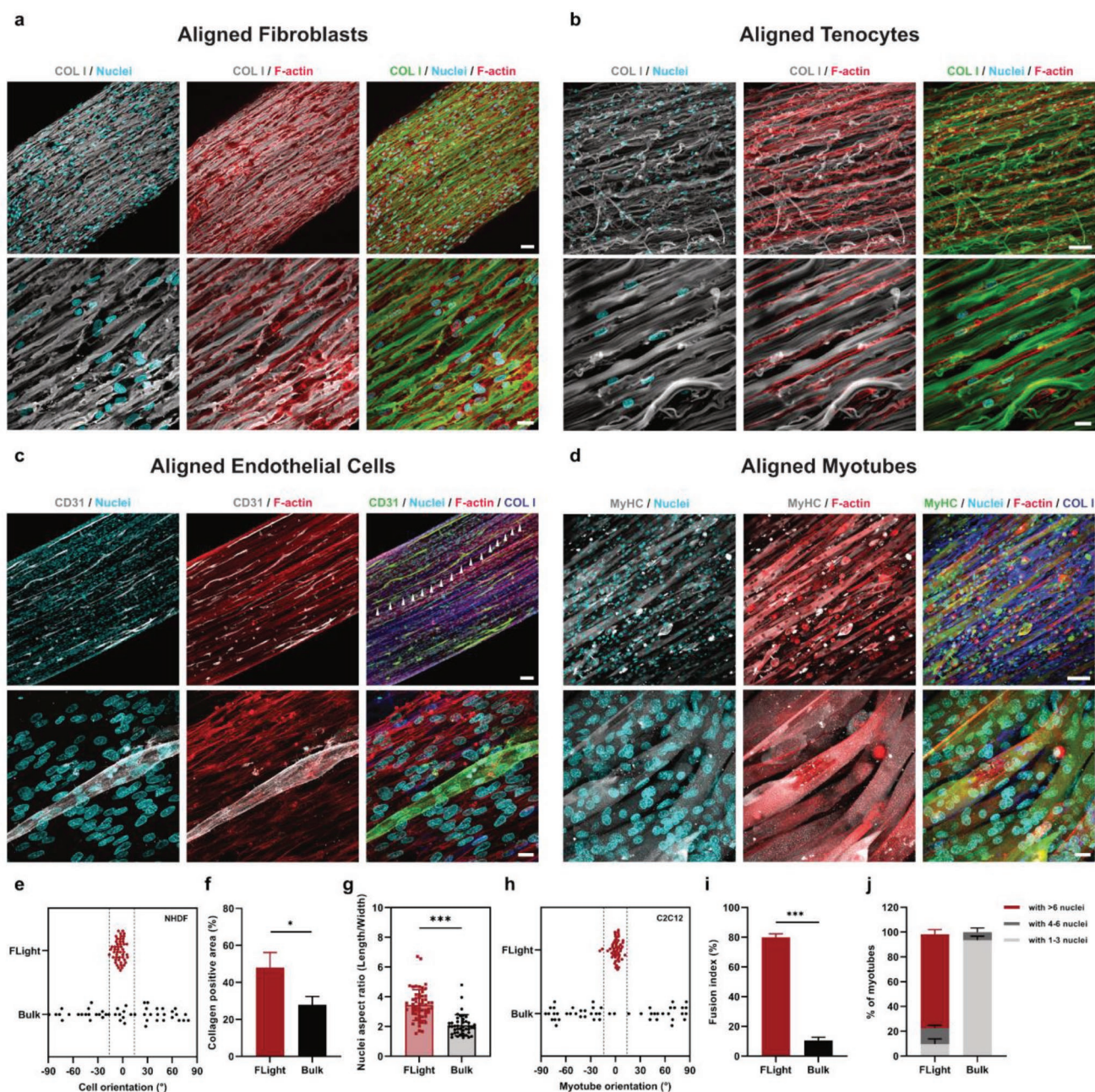


Figure 5. Cell guidance properties of microfilaments and maturation of highly aligned tissue-engineered constructs. a) Evidence of NHDFs alignment using phalloidin staining, and immunofluorescence staining of highly aligned collagen type I in FLight hydrogel constructs after 2 weeks of culture. Scale bars: 50 μm in the top panel, and 20 μm in the bottom panel. b) Alignment of HTs and collagen type I fiber in FLight hydrogel constructs at 2 weeks of culture. Scale bars: 50 and 20 μm , respectively. c) Immunofluorescence images as evidence of highly aligned vasculature in an NHDFs-HUVEC co-culture system after 2 weeks of incubation. The white arrows highlight a continuous blood capillary with length up to 1 mm. Scale bars in top and bottom panels: 100 and 20 μm , respectively. d) Immunofluorescence staining of myosin heavy chain (MyHC) and collagen type I in muscle tissue-engineered constructs after 3 weeks of culture in differentiation medium. Scale bars: 100 and 20 μm in magnified images. e) Distribution of the angle between the aligned orientation of NHDF and the parallel position to microfilaments in FLight hydrogels, and the distribution of the angle between the long axis direction of NHDF and bulk hydrogel after 2 weeks of culture. All data were collected from fluorescence images ($n = 3$). f) Ratio of collagen type I positive area in NHDFs-laden FLight hydrogels and in NHDFs-laden bulk hydrogels ($n = 3$). g) Mean value of NHDFs' nuclei aspect ratio in FLight and bulk hydrogel constructs ($n = 3$). h) Distribution of the angle between the myotubes' aligned orientation and parallel position to microfilaments in FLight tissue-engineered constructs after 3 weeks of culture in differentiation medium. All data were calculated from the fluorescence images using ImageJ ($n = 3$). i) Fusion index of myoblasts and j) ratio of nuclei number per fused myotubes to evaluate muscle maturation. All results were measured from fluorescence images ($n = 3$).

anisotropic tissue-engineered constructs. FLight offers a critical advantage over conventional strategies, which are often reliant on post-seeding of cells onto fiber-based scaffolds and substrates.^[65] The fact that these techniques merely provide a 2D microenvironment and inhomogenous cell distribution further limits their applications. For extrusion-based bioprinting strategies, a high concentration of fibrillar components and smaller nozzles are often necessary to achieve effective cell alignment, which can generate significant shear stress on cells.^[14,66–68]

2.5. FLight/Multi-FLight for Biofabrication of Complex Hydrogel Constructs

Lastly, we explored the FLight's potential to create anisotropic tissue-engineered constructs mimicking in vivo tissue structures.^[7] Varying hydrogel constructs with detailed features were produced using 2.88% w/v Gel-NB/4PEG-SH photoresin including hollow structures (Figure 6a and Figure S14, Supporting Information) and a hydrogel QR code (7 × 7 mm) with ≈220 μm feature size. Also, cell-laden tubular hydrogel structures were created, and the encapsulated NHDFs were stained with calcein-AM after 7 days of culture (Figure 6b). Monolayers of NHDFs were observed on the inner and outer walls of the tubular structures. The subsequent filling of the channels with a fluorescent-label dye (red) indicated that these tubular structures were maintained after 7 days of culture. The above results demonstrated that FLight biofabrication is a promising method for creating anisotropic hydrogel constructs with free-designed cross-sectional structures for anisotropic tissue engineering.

A multicellular/multimaterial FLight biofabrication strategy was established by performing multiple sequential projections with an exchange of bioresin between projections. Multi-FLight allows for the creation of hierarchical organization of tissues, with control over the placement of cells and matrix types. As shown in Figure 6c, multimaterial structures were achieved with two complementary projection images. With the first image, the bioresin was spatially cured to create the first part of the hydrogel structure. After removing the uncrosslinked bioresin, the second bioresin was loaded into the vial and the second complementary image was projected. As demonstrated, acellular FLight hydrogel constructs were produced using two fluorescent-labeled photoresins (Figure 6d). The CellTracker Green-labeled NHDFs were mixed with 5% w/v Gel-NB/4PEG-SH photoresin and the central cylindrical hydrogel structures were projected. The peripheral tissue-engineered constructs loaded with CellTracker Red-labeled NHDFs were created by FLight using 2.88% w/v Gel-NB/4PEG-SH photoresin. The successful encapsulation of two fluorescent-labeled cells into the designed hydrogel structure was confirmed (Figure 6e). As expected, the alignment of cells in both projected hydrogel constructs was observed after 7 days of incubation, due to the presence of microfilament structuring in hydrogel constructs.

Finally, multiple types of FLight biofabrication strategies were demonstrated, including a multidirectional FLight (Cross-FLight) and multistep FLight (Multi-FLight). In the Cross-FLight process, the second projection was performed from a different direction (1° to 90°) to the previous projection, to create hydrogel constructs containing microfilaments aligned

in multiple directions. The multidirectional microfilaments were observed in the Cross-FLight hydrogel constructs fabricated using 5% w/v fluorescent-labeled Gel-MA photoresin (Figure 6f). These unique microstructures in Cross-FLight hydrogel constructs are promising for engineering tissue constructs that need complex tissue organization and cell alignment, such as myocardial muscle tissues.^[7] The scaling-up ability of the FLight biofabrication method has been demonstrated by Multi-FLight, in which single hydrogel constructs (≈5 mm in length) can be stacked on top of each other to result in a long hydrogel construct (≈2 cm in length) featuring microfilaments throughout its entire length of the whole hydrogel constructs. Briefly, the new photoresin, which can be different from the previous photoresin, was added to the top after the last FLight process, and then the new FLight process was performed from the top of vial. In Figure 6g, a 2 cm long hydrogel construct was created, and the fusion of microfilaments from the different steps of FLight was confirmed from fluorescence images. These results demonstrated the ability of Multi-FLight biofabrication to create tissue-engineered constructs containing continuous microfilaments; and Multi-FLight offers a potential method for rapid biofabrication of human-scale muscle engineered constructs and complex tissue interfaces (i.e., muscle-tendon junction), incorporating multiple distinct morphologies/microstructures/cell types.^[32]

3. Conclusion and Future Outlook

We have demonstrated a rapid biofabrication method for creating 3D hydrogel constructs containing cell-guiding microfilaments. The alignment of four types of cells/deposited ECM was achieved by FLight biofabrication. The ultrahigh-aspect-ratio topological cues provided by the microchannels had a potent effect on cell and nuclear morphology. By synergizing with sequential projections from single or multiple directions, a multicellular/multimaterial biofabrication strategy that can mimic the hierarchical organization of anisotropic tissues was established.

Future investigation into the relationship between photochemistry/optics (e.g., molecular weight, RI changes, wavelengths, light intensity, etc.) and control of microfilaments/microchannels properties (e.g., dimension, tunable void fraction, etc.)^[69] will pave the way for broader application of this technology. For example, optimized photoresin formula including RI matching agent (e.g., iodixanol), photoabsorption dye (e.g., sunset yellow FCF (disodium 6-hydroxy-5-((4-sulfonatophenyl)diazenyl)naphthalene-2-sulfonate)), and free radical inhibitor (e.g., TEMPO (2,2,6,6-tetramethyl-1-piperidinyloxy)), all show promise to achieve better control of the slight crosslinking between microfilaments, and better projection resolution/light penetration depth with high cell concentration.^[6,70] It can be expected that FLight biofabrication of anisotropic tissues will greatly benefit from the development of photosensitive materials, such as norbornene-functionalized collagen/chitosan/fibrinogen/silk and norbornene-functionalized decellularized extracellular matrix for enhanced biocompatibility and tissue functions, or synthetic polymers like norbornene-functionalized poly(vinyl alcohol), acrylate-modified poly(ethylene glycol), PEG-SH/PEG-NB for tunable degradation rate.^[1]

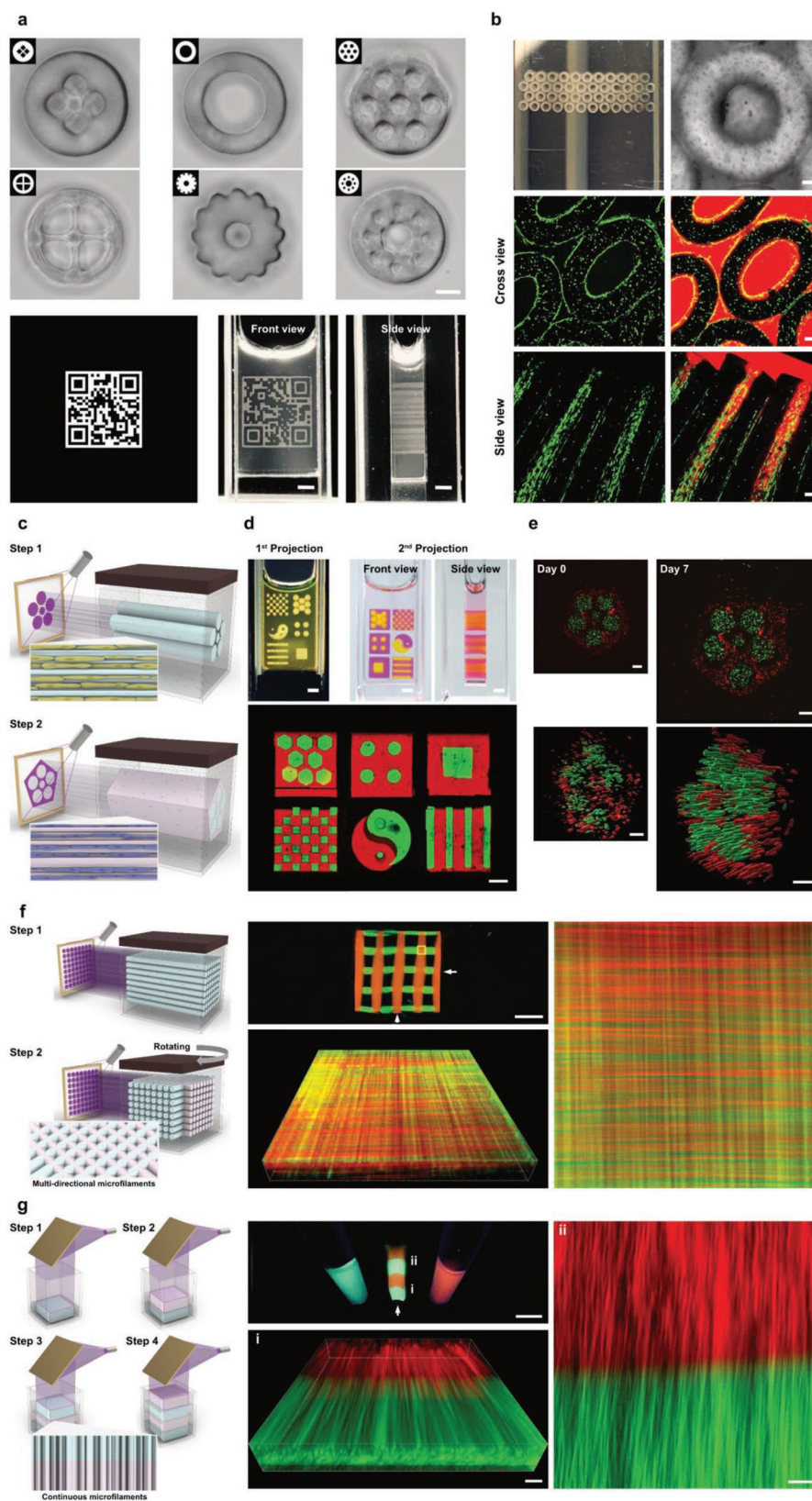


Figure 6. FLight/Multi-FLight for biofabrication of complex hydrogel constructs. a) Top: Bright-field images (cross-section views) of varying FLight hydrogel constructs created using 2.88% w/v Gel-NB/4PEG-SH photoresin. Inserts are the projection images used to fabricate hydrogel samples. Bottom: Projection images used for fabrication of a hydrogel QR code construct (7 × 7 mm), and the photographs of the hydrogel construct; a single

The FLight hydrogel constructs exhibit ideal mechanical properties that permit application of mechanical loading, which shows promise to achieve matured anisotropic tissues. As ultrahigh-aspect-ratio topological cues, microfilaments/microchannels are valuable for a better understanding of cell behavior and genomic change under mechanical confinement from a mechanobiological view. Finally, we foresee that FLight process can be used for the fabrication of acellular grafts, acting as guidance cues for the in situ regeneration of aligned tissues such as nerves.^[71]

4. Experimental Section

All chemicals were purchased from Sigma-Aldrich and cell culture reagents from Gibco unless otherwise indicated.

Synthesis of Gel-NB: The synthesis process of Gel-NB and its characterization were described in previous study:^[5] briefly, gelatin type A from porcine skin was dissolved at 10% w/v in 0.1 M pH 9 carbonate-bicarbonate buffer at 50 °C. Then, 1/5 of the total cis-5-norbornene-endo-2,3-dicarboxylic anhydride (carbic anhydride, CA) necessary to get the desired Gel:CA ratio was added to the solution. The reaction was left to proceed for 10 min under stirring prior to pH adjustment to 9 with NaOH 0.5 M solution. pH adjustment and sequential addition of CA were repeated five times every 10 min. The solution was then diluted twofold with Milli-Q water prewarmed to 40 °C and the pH adjusted to 7.4 with a solution of HCl 0.5 M. Upon centrifugation for 15 min at 3000 rcf, the supernatant was then dialyzed at 40 °C against Milli-Q water with frequent water changes for 3–4 days and finally freeze-dried.

For the photoresin preparation, the freeze-dried Gel-NB was dissolved in phosphate-buffered saline (PBS) and kept at 40 °C for 30 min. The 4PEG-SH (10 kDa, JenKem Technology) was added to the Gel-NB solution to obtain the desired SH:NB ratio (1:1). Next, a 2% w/v photoinitiator (PI) lithium phenyl-2,4,6-trimethylbenzoylphosphine (LAP) stock solution in PBS was mixed with Gel-NB/4PEG-SH solution to get a final concentration at 0.05% w/v. The photoresin was filtered by 0.45 µm filter (Filtropur S 0.45, SARSTEDT AG) and stored away from light.

Synthesis of Gel-MA and Fluorescent-Labeled Gel-MA: Gel-MA was synthesized as previously described.^[72] The degree of substitution (DS) was estimated with ¹H NMR (Bruker Ultrashield 400 MHz, 1024 scans) in D₂O (Apollo Scientific). Gel-MA lysine integration signal (2.95–3.05 ppm) was compared to unmodified gelatin lysine integration signal (2.95–3.05 ppm). Phenylalanine signal (7.2–7.5 ppm) was used as an internal reference. DS was found to be ≈45%.

Fluorescent-labeled Gel-MA was fabricated by modifying the fluorescein-5-isothiocyanate (FITC) or rhodamine B isothiocyanate

(RBITC) onto the Gel-MA. Briefly, 10% w/v of Gel-MA was first dissolved in 100 × 10⁻³ M sodium bicarbonate solution. A 0.1% w/v of FITC-dimethylformamide or rhodamine solution was then added, and the mixture was stirred at 40 °C for 6 h in the dark. After the reaction, the mixture was dialyzed against deionized water for 4 days at 30 °C to remove the unreacted monomers with subsequent freeze-drying to obtain fluorescent-labeled Gel-MA.

For the photoresin preparation, the freeze-dried Gel-MA was dissolved in PBS and kept at 40 °C for 30 min. Then, a 2% w/v LAP stock solution was mixed with Gel-MA solution to achieve a final concentration of 5% w/v Gel-MA and 0.05% w/v LAP. The photoresin was filtered by 0.45 µm filter and stored away from light.

Synthesis of HA-MA: Low-molecular-weight HA-MA ($M_w = 50\,000\text{--}70\,000$) was purchased with the DS 20–50%.

For photoresin preparation, HA-MA was dispersed in PBS and stirred at 4 °C until complete dissolution and then mixed with a 2% w/v LAP stock solution to prepare 2% w/v HA-MA and 0.05% w/v LAP solutions. The photoresin was filtered by 0.45 µm filter and stored away from light.

Synthesis of Alg-MA: Sodium alginate ($M_w > 200$ kDa, PRONOVA UP MVG, NovaMatrix) was dissolved in 25 mL of Milli-Q water to produce 1% w/v solution by continuous stirring. Methacrylic anhydride was distilled prior to use (20 eq. to hydroxyl groups, 52 mmol, 7.7 mL) and added; the formed emulsion was vigorously stirred for 24 h at room temperature. pH was frequently checked and adjusted to 7–8 with NaOH 0.5 M solution. The solution was transferred to Falcon tubes and centrifuged at 3000 rcf for 15 min to remove excess methacrylic anhydride. The aqueous phase was precipitated into ethanol and the precipitate was filtered through a fritted glass funnel (S4 porosity) and dried overnight under high vacuum. Dry Alg-MA was dissolved in Milli-Q water and then dialyzed at room temperature with frequent water changes for 3–4 days. The Alg-MA was obtained after freeze-drying. ¹H NMR spectra to determine DS were acquired using 1% w/v Alg-MA in D₂O on a Bruker spectrometer operating at a 400 MHz proton frequency. DS was found to be ≈51%.

To prepare the photoresin, the freeze-dried Alg-MA was dissolved in PBS. Then an LAP stock solution was mixed with Alg-MA solution to achieve a final concentration of 2% w/v Alg-MA and 0.05% w/v LAP. The photoresin was filtered by 0.45 µm filter before use.

Cell Culture: Tenocytes were kindly provided by Prof. Lee Ann Applegate and described previously.^[73] Human fetal progenitor tenocytes were isolated from the Achilles tendon of a male 14 week gestation organ donation according to a protocol approved by an ethics committee. University Hospital of Lausanne (CHUV), Ethics Committee Protocol No. 62/07: 14-week gestation organ donation, registered under the Federal Transplantation Program and its DAL (Department of Musculoskeletal Medicine) Biobank complying with the laws and regulations. NHDFs were isolated from juvenile foreskin skin biopsies. The biopsies were obtained under parental informed consent and their use for research purposes was approved by the Ethical Committee

pixel in the QR code image corresponds to about 220 µm. Scale bars: 200 µm in BF image and 2 mm in photograph. b) Top: Photograph and bright-field image of cell-laden tubular hydrogel constructs fabricated using 2.88% w/v Gel-NB/4PEG-SH bioresin. Middle and bottom: Fluorescence images of tubular constructs from front view and side view. The encapsulated NHDFs were labeled by Calcein-AM, and the RhoD-labeled Dextran was added into tubular hydrogel constructs after 7 days of culture. Scale bars: 100 µm. c) Schematic illustration of multicellular/multimaterial FLight for heterogeneous biofabrication of anisotropic tissue-engineered constructs. d) Photographs and full scanned fluorescence image of varying hydrogel constructs achieved by multimaterial FLight process using 5% w/v FITC- and Rhod-labeled Gel-MA photoresin. Scale bars: 2 mm in the photograph and 1 mm in the fluorescence image. e) Fluorescence images of hydrogel constructs fabricated by multimaterial FLight process on day 0 and day 7. The NHDFs were labeled by CellTracker Green or Red, and encapsulated in the hydrogel constructs fabricated using 5% and 2.88% w/v Gel-NB/4PEG-SH photoresin, respectively. The side view of cell alignment after 7 days of culture was generated by Imaris from a full scanned 3D fluorescence image. Scale bars: 200 µm in all fluorescence images. f) Schematic illustration of multidirectional FLight process (Cross-FLight) and the fluorescence images of the aligned microfilaments in the hydrogel constructs. The white arrows indicate the directions of microfilaments (i.e., the directions of FLight projections) in hydrogel constructs. The zoom-in images show the microstructure of the microfilaments in the cross-zone from the yellow squares. Scale bars: 500 µm in photographs and 20 µm in microscopy images of microfilaments. g) Schematic illustration of multistep FLight process (Multi-FLight) for biofabrication of long hydrogel constructs and the confocal images of the fusion of the microfilaments between the different steps of FLight. The white arrow indicates the direction of the FLight projection (i.e., multistep FLight repeated in the same direction). Scale bars: 1 cm in the photographs and 20 µm in microscopy images of the interfaces (i and ii).

of Canton Zurich (BASEC-Request-Nr. 2018-00269). Tenocytes and NHDFs were cultured in Falcon Cell Culture Multi-Flask (TC 5-layer, 875 cm²) with DMEM+GlutaMAX-I + 10% w/v fetal bovine serum (FBS) + 10 µg mL⁻¹ Antibiotic-Antimycotic (Anti-Anti). Myoblasts (C2C12) were obtained from ATCC and cultured in Dulbecco's modified Eagle medium (DMEM) medium + 10% v/v FBS + 10 µg mL⁻¹ Anti-Anti for cell proliferation. Cells were passaged at 90% confluence and detached using 0.25% Trypsin/ethylenediaminetetraacetic acid. For C2C12 differentiation, the cell-laden hydrogels were incubated in differentiation medium composed of DMEM + 2% v/v horse serum + 1% v/v Insulin-Transferrin-Selenium (ITS+, Corning) + 10 µg mL⁻¹ gentamicin. Samples were cultured in a 35 mm petri dish (PS 60/15 MM, Greiner Bio-One) with frequent medium changes. HUVECs were purchased from Lonza and cultured in endothelial cell growth medium-2 BulletKit (EGM-2, Lonza). For the HUVEC-NHDF co-culture system in hydrogel construct, HUVEC and NHDFs were mixed at a ratio of 1:2 in the photoresin to prepare the biophotoresin. The fabricated cell-laden hydrogel samples were transferred into 6 well plates and cultured in a mixed medium (DMEM:EGM-2 as 1:1).

Preparation of Bioresin: Photoresins were prepared as indicated above. A 0.2 µm filter (Filterpur S 0.2, SARSTEDT AG) was used to sterilize the photoresins and remove potentially scattering particles. The NHDFs and HTs were resuspended in photoresins at a concentration of 1 million cells mL⁻¹. The C2C12 was mixed with photoresins at 2 million cells mL⁻¹. For NHDFs-HUVEC co-culture, two types of cells were mixed at a ratio of 2:1 at a concentration of 1 million cells mL⁻¹ in photoresins.

Design of Projection Images for FLIGHT Biofabrication: Projection images were created using Affinity Photo (Affinity Suite 1.9, Serif Europe Ltd.) with a fixed resolution of 1024 × 768 pixels. The images were grayscale, with a pure white color corresponding to 100% light intensity (≈62.5 mW cm⁻²). The width of each pixel in the projection image was equal to about 27 µm. The patterns were corrected by 90° as they were projected, with a 90° rotation to the vials and cuvettes. The projection images were then exported as PNG files.

Assemblage of Standard Köhler Illumination System: All components for assembling a standard Köhler illumination system were bought from Thorlabs if not otherwise clarified, including the light source (M405L4). The assembly and alignment protocols were described in a previous study.^[37] Light intensity in front of the cuvette was measured after each adjustment of field diameter and/or aperture diameter using a power meter.

FLIGHT Biofabrication: (Bio)photoresins were prepared as described above and transferred to sterilized cuvettes or glass vials. The Gel-NB/4PEG-SH and Gel-MA (bio)photoresins were allowed to thermally gel at 4 °C for 15 min. For highly viscous photoresins or nonthermoreversible photoresins (i.e., HA-MA, Alg-MA), the above steps were skipped. The FLIGHT projections were performed a tomographic volumetric printer (Tomolite Ver. 1.0, Readily3D SA) without rotation of the photoresin container, and the light intensity was approximately 62.5 mW cm⁻². The projection times were calculated based on the light intensity and the light doses required for the crosslinking of each photoresin. The projection images were loaded into the software (Apparite, Readily3D SA) before starting the projection. Uncrosslinked (bio)photoresin was washed away using PBS prewarmed to 37 °C. The projected constructs were removed using a sterile spatula and transferred into PBS or culture medium.

Compression Modulus Measurements: All samples were prepared as cylindrical models with a diameter of 5 mm and height of 4 mm. A circular projection image of 185 pixels in diameter was used to prepare the FLIGHT hydrogel samples. Bulk hydrogel samples (control group) were generated by filling photoresin into polymethylsiloxane molds (5 mm inner diameter and 4 mm height) before UV crosslinking. Samples were tested by unconfined uniaxial compression using TA.XTplus Texture Analyzer (Stable Micro systems). A 500 g load cell and a flat plate probe (15 mm) were used. A 0.2 g preload was applied to ensure that the samples were in full contact with the plates. Samples were compressed to a final strain of 50% at a rate of 0.01 mm s⁻¹. Elastic compressive modulus was calculated by linear fitting of initial linear

region (0.5–5%) of the stress–strain curve. The tests were carried out at 25 °C and repeated three times.

Tensile Tests: All samples were prepared as hydrogel strands with a diameter of 1 mm. A circular matrix (8 × 8) image of 37 pixels in diameter was loaded to FLIGHT system. Bulk hydrogel samples were created by pressing the bulk gel through a grid (1 mm, micrometer-sized apertures) after thermoreversible gelation of photoresin. Microstrands were then crosslinked under a UV lamp using the same light dose as for the FLIGHT process. Tensile tests were performed by Texture Analyzer equipped with a 500 g load cell using miniature tensile grips and a 0.1 g preload was applied before tension. All samples were stretched at a speed of 0.1 mm s⁻¹ until fracture. The loading–unloading curves were measured at a tensile strain of 0–50%, with a tension rate of 0.1 mm s⁻¹ over 12 time cycles.

Cell Viability: Hydrogel constructs were washed three times with PBS after 0, 3, and 7 days of culture and then incubated for 45 min in FluoroBrite™ DMEM supplemented with 1:2000 calcein-AM (Invitrogen), 1:1000 Hoechst 33342 (Invitrogen), and 1:500 propidium iodide (PI, Fluka). Fluorescence imaging was performed with a confocal laser scanning microscope (CLSM; Fluoview 3000, Olympus) after three times washing in medium. Z-stacks scanning was acquired from the surface of constructs at 5 µm steps 200 µm into the constructs. The z-projection images were analyzed with Fiji ImageJ. The above experiment was repeated three times, with the viability of each sample averaged over three images of randomly chosen areas.

CellTracker Dye Loading: CellTracker Green dye CMFDA (Invitrogen) and CellTracker Red dye CMTPX were applied to NHDFs in serum-free medium at a working concentration of 10 × 10⁻⁶ M. Cells were transferred to the incubator at 37 °C for 1 h and then washed with PBS three times for subsequent experiments.

Immunofluorescence Staining: Cell-laden hydrogel constructs were washed with PBS three times after 7 days of culture and fixed in 4% paraformaldehyde for 30 min at 25 °C. The strands were permeabilized with 0.2% Triton-X100 in PBS for 30 min before blocking with 1% v/v bovine serum albumin (BSA) in PBS for 1 h. The constructs were then incubated with primary antihuman collagen I antibody (ab138492, Abcam) 1/500 diluted in BSA-PBS at 4 °C for 12 h. Next, the samples were washed three times with PBS, incubated with 1/200 diluted secondary antibody (Goat anti-Rabbit Alexa Fluor 488, Invitrogen), Hoechst 33342, and pre-prepared phalloidin-tetramethylrhodamine B isothiocyanate working solution (0.13 µg mL⁻¹, P1951) in BSA-PBS for 2 h at 4 °C. C2C12 constructs were incubated with 1/20 diluted primary antihuman myosin heavy chain antibody (MF-20, DSHB) and 1/500 diluted collagen I antibody for 12 h at 4 °C. The samples were then incubated with 1/200 diluted secondary antibody (Goat anti-Rabbit Alexa Fluor 647, Goat anti-Mouse Alexa Fluor Plus 488), phalloidin-tetramethylrhodamine B isothiocyanate working solution, and Hoechst for 2 h at 4 °C. Samples were washed with PBS before imaging on CLSM. NHDFs encapsulated in tubular constructs, encapsulated in fluorescence Gel-MA, or seeded on the surface were stained by calcein-AM for 1 h. Tubular constructs were then perfused with 40 kDa tetramethylrhodamine isothiocyanate-dextran (TRITC-dextran) for 10 min before confocal imaging.

RNA Isolation and Quantitative Reverse Transcription Polymerase Chain Reaction: NHDFs were encapsulated into hydrogel samples fabricated using 2.88% w/v Gel-NB/4PEG-SH photoresin. The tissue samples were homogenized with tissue grinders and incubated with NucleoZOL (MACHERY-NAGEL) at room temperature for 10 min. DNase-free water was added to the samples and mixtures were centrifuged for 10 min at 12 000 rcf. The supernatants were mixed with 70% EtOH and transferred to the RNeasy mini kit (Qiagen) column to extract the total RNA. An A260/280 ratio of between 1.8 and 2.1 was accepted as adequate quality for the RNA samples. The isolated RNA was transcribed to complementary DNA following the instruction of GoScript Reverse Transcriptase kit (Promega). The relative gene expression levels were determined on real-time PCR System (QuantStudio 5, Applied Biosystems) with the SYBR Green PCR Master Mix (Promega). The GAPDH housekeeper gene was used as an internal control for the normalization of RNA levels.

3D Image Reconstruction: The 3D images obtained using confocal microscopy were imported into Imapris 9.2.1 for reconstruction of the 3D model. The measurements in this work were performed by surface and statistic functions.

Statistical Analysis: Statistical analysis was performed using GraphPad Prism (x64, v. 9.2.0) and unpaired *t*-tests. Alpha was set to 0.05 and differences between two experimental groups were judged to have statistical significance at **p* < 0.05, ***p* < 0.01, and ****p* < 0.005; *ns* represents “no significant difference” between two groups.

Supporting Information

Supporting Information is available from the Wiley Online Library or from the author.

Acknowledgements

D.R. and R.R. contributed equally to this work. M.Z.W. acknowledges ETH Grant application ETH-38 19-1 and Innosuisse funding application no. 55019.1 IP-ENG for their kind support. P.C. acknowledges a Marie Skłodowska Curie fellowship (grant number 101024341). D.R. acknowledges Swiss National Science Foundation project grant 205321_179012. P.D. acknowledges the BPM-Matlab tool kindly shared by DTU for the light beam simulations. The authors thank Dr. Thomas Biedermann (Tissue Biology Research Unit, University Children's Hospital Zurich) for kindly providing fibroblasts. The authors further acknowledge the assistance from ETH (ScopeM) imaging facility. The authors acknowledge Pierre Guillon for his great contribution to the design of schematic illustrations.

Open access funding provided by Eidgenössische Technische Hochschule Zurich.

Conflict of Interest

D.L. and P.D. are employed by Readily3D and hold shares.

Data Availability Statement

The data that support the findings of this study are available from the corresponding author upon reasonable request.

Keywords

cell guidance, microstructure, muscle tissues, optical modulation instability, photo-crosslinking

Received: May 12, 2022
Revised: September 7, 2022
Published online: October 9, 2022

- [1] M. Lee, R. Rizzo, F. Surman, M. Zenobi-Wong, *Chem. Rev.* **2020**, *120*, 10950.
[2] K. S. Lim, J. H. Galarraga, X. Cui, G. C. J. Lindberg, J. A. Burdick, T. B. F. Woodfield, *Chem. Rev.* **2020**, *120*, 10662.
[3] L. Moroni, J. A. Burdick, C. Highley, S. J. Lee, Y. Morimoto, S. Takeuchi, J. J. Yoo, *Nat. Rev. Mater.* **2018**, *3*, 21.
[4] P. N. Bernal, P. Delrot, D. Loterie, Y. Li, J. Malda, C. Moser, R. Levato, *Adv. Mater.* **2019**, *31*, 1904209.

- [5] R. Rizzo, D. Ruetsche, H. Liu, M. Zenobi-Wong, *Adv. Mater.* **2021**, *33*, 2102900.
[6] P. N. Bernal, M. Bouwmeester, J. Madrid-Wolff, M. Falandt, S. Florczak, N. G. Rodriguez, Y. Li, G. Großbacher, R.-A. Samsom, M. van Wolferen, L. J. W. van der Laan, P. Delrot, D. Loterie, J. Malda, C. Moser, B. Spee, R. Levato, *Adv. Mater.* **2022**, *34*, 2110054.
[7] N. Khuu, S. Kheiri, E. Kumacheva, *Trends Chem.* **2021**, *3*, 1002.
[8] J. Xing, N. Liu, N. Xu, W. Chen, D. Xing, *Adv. Funct. Mater.* **2022**, *32*, 2110676.
[9] J. Zhang, Q. Hu, S. Wang, J. Tao, M. Gou, *Int. J. Bioprint.* **2020**, *6*, 19.
[10] U. Streppel, D. Michaelis, R. Kowarschik, A. Bräuer, *Phys. Rev. Lett.* **2005**, *95*, 73901.
[11] S. Jana, S. K. L. Levengood, M. Zhang, *Adv. Mater.* **2016**, *28*, 10588.
[12] Y. Luo, J. Li, B. Li, Y. Xia, H. Wang, C. Fu, *Front. Cell Dev. Biol.* **2021**, *9*, 731170.
[13] C. Mueller, M. Trujillo-Miranda, M. Maier, D. E. Heath, A. J. O'Connor, S. Salehi, *Adv. Mater. Interfaces* **2021**, *8*, 2001167.
[14] A. Schwab, C. Hélayr, R. G. Richards, M. Alini, D. Eglin, M. D'Este, *Mater. Today Bio* **2020**, *7*, 100058.
[15] J. C. Rose, D. B. Gehlen, T. Haraszti, J. Köhler, C. J. Licht, L. De Laporte, *Biomaterials* **2018**, *163*, 128.
[16] J. C. Rose, M. Cámara-Torres, K. Rahimi, J. Köhler, M. Möller, L. De Laporte, *Nano Lett.* **2017**, *17*, 3782.
[17] P. Viswanathan, M. G. Ondeck, S. Chirasatitsin, K. Ngamkham, G. C. Reilly, A. J. Engler, G. Battaglia, *Biomaterials* **2015**, *52*, 140.
[18] Y. Hu, J.-O. You, J. Aizenberg, *ACS Appl. Mater. Interfaces* **2016**, *8*, 21939.
[19] P. Jevtić, L. J. Edens, L. D. Vuković, D. L. Levy, *Curr. Opin. Cell Biol.* **2014**, *28*, 16.
[20] C. Uhler, G. V. Shivashankar, *Nat. Rev. Mol. Cell Biol.* **2017**, *18*, 717.
[21] Y. Xu, G. A. C. Murrell, *Clin. Orthop. Relat. Res.* **2008**, *466*, 1528.
[22] A. Islam, M. Younesi, T. Mbimba, O. Akkus, *Adv. Healthcare Mater.* **2016**, *5*, 2237.
[23] A. Dede Eren, A. Vasilevich, E. D. Eren, P. Sudarsanam, U. Tuvshindorj, J. de Boer, J. Foolen, *Tissue Eng., Part A* **2020**, *27*, 1023.
[24] D. Kip, M. Soljagic, M. Segev, E. Eugenieva, D. N. Christodoulides, *Science* **2000**, *290*, 495.
[25] I. D. Hosein, *Chem. Mater.* **2020**, *32*, 2673.
[26] S. Biria, P. P. A. Malley, T. F. Kahan, I. D. Hosein, *J. Phys. Chem. C* **2016**, *120*, 4517.
[27] M. Anyfantakis, B. Loppinet, G. Fytas, S. Pispas, *Opt. Lett.* **2008**, *33*, 2839.
[28] Y. Fang, L. Ouyang, T. Zhang, C. Wang, B. Lu, W. Sun, *Adv. Healthcare Mater.* **2020**, *9*, 2000782.
[29] N. Annabi, J. W. Nichol, X. Zhong, C. Ji, S. Koshy, A. Khademhosseini, F. Dehghani, *Tissue Eng., Part B* **2010**, *16*, 371.
[30] G. C. Engelmayr, M. Cheng, C. J. Bettinger, J. T. Borenstein, R. Langer, L. E. Freed, *Nat. Mater.* **2008**, *7*, 1003.
[31] P. Chansoria, E. L. Etter, J. Nguyen, *Trends Biotechnol.* **2022**, *40*, 338.
[32] B. Charvet, F. Ruggiero, D. Le Guellec, *Muscles. Ligaments Tendons J.* **2012**, *2*, 53.
[33] M. Veetikazhy, A. Kragh Hansen, D. Marti, S. Mark Jensen, A. Lykke Borre, E. Ravn Andresen, K. Dholakia, P. Eskil Andersen, *Opt. Express* **2021**, *29*, 11819.
[34] P. Chansoria, S. Asif, K. Polkoff, J. Chung, J. A. Piedrahita, R. A. Shirwaiker, *ACS Biomater. Sci. Eng.* **2021**, *7*, 5175.
[35] E. Prince, E. Kumacheva, *Nat. Rev. Mater.* **2019**, *4*, 99.
[36] J. K. Mouw, G. Ou, V. M. Weaver, *Nat. Rev. Mol. Cell Biol.* **2014**, *15*, 771.
[37] J. Madrid-Wolff, M. Forero-Shelton, *Biophysicist* **2020**, *1*, 10.
[38] J. Visser, F. P. W. Melchels, J. E. Jeon, E. M. van Bussel, L. S. Kimpton, H. M. Byrne, W. J. A. Dhert, P. D. Dalton, D. W. Huttmacher, J. Malda, *Nat. Commun.* **2015**, *6*, 6933.
[39] Y. Huang, D. R. King, T. L. Sun, T. Nonoyama, T. Kurokawa, T. Nakajima, J. P. Gong, *Adv. Funct. Mater.* **2017**, *27*, 1605350.
[40] C. Rinoldi, M. Costantini, E. Kijeńska-Gawrońska, S. Testa, E. Fornetti, M. Heljak, M. Ćwiklińska, R. Buda, J. Baldi, S. Cannata,

- J. Guzowski, C. Gargioli, A. Khademhosseini, W. Swieszkowski, *Adv. Healthcare Mater.* **2019**, *8*, 1801218.
- [41] C. Rinoldi, A. Fallahi, I. K. Yazdi, J. Campos Paras, E. Kijeńska-Gawrońska, G. Trujillo-de Santiago, A. Tuoheti, D. Demarchi, N. Annabi, A. Khademhosseini, W. Swieszkowski, A. Tamayol, *ACS Biomater. Sci. Eng.* **2019**, *5*, 2953.
- [42] A. K. Gaharwar, I. Singh, A. Khademhosseini, *Nat. Rev. Mater.* **2020**, *5*, 686.
- [43] M. P. Nikolova, M. S. Chavali, *Bioact. Mater.* **2019**, *4*, 271.
- [44] M. Zhu, W. Li, X. Dong, X. Yuan, A. C. Midgley, H. Chang, Y. Wang, H. Wang, K. Wang, P. X. Ma, H. Wang, D. Kong, *Nat. Commun.* **2019**, *10*, 4620.
- [45] K. Wolf, M. te Lindert, M. Krause, S. Alexander, J. te Riet, A. L. Willis, R. M. Hoffman, C. G. Figdor, S. J. Weiss, P. Friedl, *J. Cell Biol.* **2013**, *201*, 1069.
- [46] M. Egerbacher, S. Gabner, S. Battisti, S. Handschuh, *J. Anat.* **2020**, *236*, 165.
- [47] E. M. McNally, A. R. Demonbreun, *Science* **2021**, *374*, 262.
- [48] J. Irianto, Y. Xia, C. R. Pfeifer, A. Athirasala, J. Ji, C. Alvey, M. Tewari, R. R. Bennett, S. M. Harding, A. J. Liu, R. A. Greenberg, D. E. Discher, *Curr. Biol.* **2017**, *27*, 210.
- [49] M. Chiquet, L. Gelman, R. Lutz, S. Maier, *Biochim. Biophys. Acta, Mol. Cell Res.* **2009**, *1793*, 911.
- [50] M. D'Urso, N. A. Kurniawan, *Front. Bioeng. Biotechnol.* **2020**, *8*, 609653.
- [51] B. Roy, L. Yuan, Y. Lee, A. Bharti, A. Mitra, G. V. Shivashankar, *Proc. Natl. Acad. Sci. USA* **2020**, *117*, 10131.
- [52] A. Wahlsten, D. Rüttsche, M. Nanni, C. Giampietro, T. Biedermann, E. Reichmann, E. Mazza, *Biomaterials* **2021**, *273*, 120779.
- [53] J. Kohler, C. Popov, B. Klotz, P. Alberton, W. C. Prall, F. Haasters, S. Müller-Deubert, R. Ebert, L. Klein-Hitpass, F. Jakob, M. Schieker, D. Docheva, *Aging Cell* **2013**, *12*, 988.
- [54] G.-C. Dai, Y.-J. Li, M.-H. Chen, P.-P. Lu, Y.-F. Rui, *World J. Stem Cells* **2019**, *11*, 677.
- [55] J. Swift, I. L. Ivanovska, A. Buxboim, T. Harada, P. C. D. P. Dingal, J. Pinter, J. D. Pajerowski, K. R. Spinler, J.-W. Shin, M. Tewari, F. Rehfeldt, D. W. Speicher, D. E. Discher, *Science* **2013**, *341*, 1240104.
- [56] Y. Fu, P. Wan, J. Zhang, X. Li, J. Xing, Y. Zou, K. Wang, H. Peng, Q. Zhu, L. Cao, X. Zhai, *Front. Cell Dev. Biol.* **2021**, *9*, 741060.
- [57] L. Wang, X. You, S. Lotinun, L. Zhang, N. Wu, W. Zou, *Nat. Commun.* **2020**, *11*, 282.
- [58] M. A. Fernandez-Yague, A. Trotier, S. Demir, S. A. Abbah, A. Larrañaga, A. Thirumaran, A. Stapleton, S. A. M. Tofail, M. Palma, M. Kilcoyne, A. Pandit, M. J. Biggs, *Adv. Mater.* **2021**, *33*, 2008788.
- [59] T. Zhou, B. Gao, Y. Fan, Y. Liu, S. Feng, Q. Cong, X. Zhang, Y. Zhou, P. S. Yadav, J. Lin, N. Wu, L. Zhao, D. Huang, S. Zhou, P. Su, Y. Yang, *eLife* **2020**, *9*, e52779.
- [60] H. Laronha, J. Caldeira, *Cells* **2020**, *9*, 1076.
- [61] A. Padhi, K. Singh, J. Franco-Barraza, D. J. Marston, E. Cukierman, K. M. Hahn, R. K. Kapania, A. S. Nain, *Commun. Biol.* **2020**, *3*, 390.
- [62] A. S. Abhilash, B. M. Baker, B. Trappmann, C. S. Chen, V. B. Shenoy, *Biophys. J.* **2014**, *107*, 1829.
- [63] D. Pei, M. Wang, W. Li, M. Li, Q. Liu, R. Ding, J. Zhao, A. Li, J. Li, F. Xu, G. Jin, *Acta Biomater.* **2020**, *112*, 202.
- [64] B. Roy, S. Venkatachalapathy, P. Ratna, Y. Wang, D. S. Jokhun, M. Nagarajan, G. V. Shivashankar, *Proc. Natl. Acad. Sci. USA* **2018**, *115*, E4741.
- [65] I. Calejo, C. J. Labrador-Rached, M. Gomez-Florit, D. Docheva, R. L. Reis, R. M. A. Domingues, M. E. Gomes, *Adv. Healthcare Mater.* **2022**, *11*, 2102863.
- [66] A. Blaeser, D. F. Duarte Campos, U. Puster, W. Richtering, M. M. Stevens, H. Fischer, *Adv. Healthcare M* **2016**, *5*, 326.
- [67] H. Kim, J. Jang, J. Park, K.-P. Lee, S. Lee, D.-M. Lee, K. H. Kim, H. K. Kim, D.-W. Cho, *Biofabrication* **2019**, *11*, 035017.
- [68] H. Liu, S. Kitano, S. Irie, R. Levato, M. Matsusaki, *Adv. Biosyst.* **2020**, *4*, 2000038.
- [69] A. Bogris, N. A. Burger, K. G. Makris, B. Loppinet, G. Fytas, *ACS Photonics* **2022**, *9*, 722.
- [70] C. C. Cook, E. J. Fong, J. J. Schwartz, D. H. Porcincula, A. C. Kaczmarek, J. S. Oakdale, B. D. Moran, K. M. Champley, C. M. Rackson, A. Muralidharan, R. R. McLeod, M. Shusteff, *Adv. Mater.* **2020**, *32*, 2003376.
- [71] M. G. Tupone, M. d'Angelo, V. Castelli, M. Catanesi, E. Benedetti, A. Cimmini, *Front. Bioeng. Biotechnol.* **2021**, *9*, 639765.
- [72] B. Kessel, M. Lee, A. Bonato, Y. Tinguely, E. Tosoratti, M. Zenobi-Wong, *Adv. Sci.* **2020**, *7*, 2001419.
- [73] A. Laurent, P. Abdel-Sayed, A. Grognez, C. Scaletta, N. Hirt-Burri, M. Michetti, A. S. de Buys Roessingh, W. Raffoul, P. Kronen, K. Nuss, B. von Rechenberg, L. A. Applegate, S. E. Darwiche, *Biomedicines* **2021**, *9*, 380.